Electronic Properties of F/Zr Co-doped Anatase TiO_2 Photocatalysts from GGA + U calculations

Run Long, Niall J. English*

The SEC Strategic Research Cluster and the Centre for Synthesis and Chemical Biology, School of Chemical and Bioprocess Engineering, University College Dublin, Belfield, Dublin 4, Ireland.

Abstract: The energetic and electronic properties of F and/or Zr-doped anatase TiO_2 are investigated by first-principles calculations. For F-doping, reduced Ti^{3+} ions are formed and Ti orbitals lie slightly below the conduction band, leading to band gap narrowing. For Zr-doping, Zr 4d orbitals reside well into the conduction band, with essentially no band gap change. For F/Zr–codoping, the electronic structure is similar to that for F–monodoping, **where Ti^{3+} gap states are induced by both the oxygen vacancy and F dopant.** The influence of oxygen vacancies indicates that interplay between dopants and oxygen vacancies is key for improvement of photocatalytic activity. The theoretical findings present a reasonable explanation of recent experimental results.

Keywords: F/Zr codoping, oxygen vacancy, electronic structure, TiO_2

* Corresponding author: Email: niall.english@ucd.ie, Tel. +353-1-716 1646, Fax: +353-1-716 1177

1. Introduction

TiO_2 has received intense attention due to its low cost, non-toxicity, long-term stability and high oxidative power; this would render it one of the most promising materials in a wide range of technical fields, such as photocatalytic degradation of pollutants and photoelectrochemical conversion of solar energy [1, 2]. However, as a wide-band gap semiconductor (e.g., around 3.20 eV for anatase), TiO_2 can be only activated under UV-light irradiation, which accounts for only a small proportion (about 5%) of solar energy. Further, its photoexcited electron-hole pairs tend to recombine easily, which serves to limit further its utility as a photcatalyst. Therefore, in order to obtain highly effective photocatalysts, there has been a large focus on experimental attempts to 'engineer' the band gap of TiO_2 via doping with metals and non-metals [3-12]. In recent decades, $\mathbf{Ti_{1-x}Zr_xO_2}$ solid solutions have been studied intensively for enhanced photocatalysis and it has been proposed that substitutional Zr^{4+} in place of Ti^{4+} would increase surface area, thermal stability and surface acidity [13, 14]. However, the solubility of Zr in TiO_2 is low, and Zr doping could destabilise the host TiO_2 lattice, limiting the photoactivity [13]. On the other hand, $TiO_{2-x}F_x$ has also attracted much attention both experimentally and theoretically for improving photocatalytic performance, not only under UV irradiation [15] but also that of visible-light [16]. Todorova et al. [17] have also reported F ions' incorporation into the TiO_2 lattice and attributed this to stronger absorption in the UV-visible region due to the presence of F^- ions which favour formation of the anatase phase and improve the crystallinity of TiO_2 without changes in the band gap. On the other hand, Yamaki

et al. [18] have performed theoretical calculations of F-doped TiO_2 and reported modifications in the conduction band edge and the introduction of impurity states near its bottom. Some previous theoretical studies [8, 19] have shown that F can neither narrow the band gap nor introduce impurities states into F-doped TiO_2 using standard density functional theory (DFT) calculations. However, Di Valentin et al. [20] have shown recently more correct physical results and behaviour of F-doped TiO_2 using hybrid functional and DFT+U calculations, in which F substitution of O will reduce one Ti^{4+} to Ti^{3+} and induce Ti 3d states below the bottom of the conduction band, which is similar to the effect of an oxygen vacancy. Since Zr^{4+} incorporation inhibits the crystallization and ripening of anatase nanocrystals and F^- ions promote the formation of this crystalline phase, Liu et al. [21] have synthesized F/Zr-codoped anatase TiO_2 and reported that synergetic effects are associated with electron transfer-mediated charge compensation between F/Zr impurities. **Recently,** there are many theoretical papers focused on explaining the microelectronic mechanisms of either monodoping by non-metal elements [8, 18, 19] or co-doping by non-metal and metal elements [12b, 22-25]. **In particular, Sanz et al's work from both theory and experiment on the (N, Au)-codoped TiO_2 surface has shown significant synergistic effects on photocatalytic activity and stabilization relative to N-monodoping, owing to electron transfer from Au 6s orbitals to N 2p states, which also serves to increase the Au-surface adhesion energy. Moreover, (N, Au)-codoped TiO_2 was found to be active for thermal dissociation of water and the production of H_2 through the water-gas shift reaction. It has been predicted**

that the interaction between Au and N also stabilizes the implantation of N in the SrO- and TiO-terminated surfaces of $SrTiO_3$ or in ZnO [12b]. However, to date, there are no related theoretical studies investigating the effects of F/Zr codoping. To understand the microscopic mechanisms of F/Zr co-doping on both geometrical structure and electronic properties, theoretical analysis by first-principles calculations is a valuable tool. Therefore, it is desirable to investigate the origins of modifications to the band structure and the enhancement of photocatalytic activity of F/Zr-doped TiO_2. Further, when anatase TiO_2 is codoped with Zr^{4+} and F^- ions, the preservation of charge balance is compensated by the creation of an oxygen vacancy. Therefore, it is both instructive and desirable to compare electronic structure properties with and without oxygen vacancies in F/Zr-codoped TiO_2.

A theoretical description of the localized atomic-like Ti 3d states induced by F ions or in the presence of oxygen vacancies is unable to provide satisfactory results in terms of either the local density approximation (LDA) or generalized gradient approximation (GGA), owing to the well-known band gap problem and the insufficient cancellation of the self-interaction energy. DFT+U methods can improve partially the prediction of the band gap, and are becoming increasing popular for the study of the electronic structures of semiconductors, and tend to produce more accurate results than those of standard DFT when used appropriately [20]. The present study focuses on studying the energetic and electronic structure of (co-)doped anatase using DFT calculations employing the GGA + U method, and attempts to elucidate the origin of changes in electronic structure and synergistic effects of F/Zr codoping

vis-à-vis F- or Zr-monodoping. We also consider here the interplay between dopants and oxygen vacancies on the electronic structure of defective TiO_2. Our theoretical analysis points out that high photocatalytic activity of F/Zr-codoped TiO_2 may stem from the creation of oxygen vacancies.

2. Methodology and Systems

All of the spin-polarized DFT calculations were performed using projector augemented wave (PAW) pseudopotentials as implanted in the Vienna *ab initio* Simulation Package [26, 27] (VASP). The Perdew-Burke-Ernzerhof parameterization of the generalized gradient approximation (GGA) [28] was adopted for the exchange-correlation potential. The electron wave function was expanded in plane -wave cutoff energy of 400 eV **and the optimized lattice constants agreed well with the experimental values. Increasing the cutoff energy up to 500eV led to a large disparity in lattice constants vis-à-vis experimental values. The Brillouin-zone integrations were performed using** Monkhorst–Pack **grids** [29]. A 2 × 2 × 2 *k*-mesh was used for geometry optimization and a substantially more dense *k*-mesh of 4 × 4 × 4 was used for electronic property calculations **because a cubic-like 3×3×1 anatase supercell was used in this study.** Both atomic positions and cell parameters were optimized with the GGA method until the residual forces were below 0.01 eV/Å. The DFT + U [30] approach introduces an on-site correction in order to describe systems with localized d and f electrons, which can produce better band gaps in comparison to experimental results. Here, effective on-site Coulomb interactions U (U = U' –J) for

Ti 3d were used to obtain the correct band gap. U' and J represent the energy cost of adding an extra electron at a particular site and the screened exchange energy, respectively. **Here, U = 5.0 eV was used on Zr 4d electrons.** A**lthough the DFT+U approach yields a more accurate band gap, the accuracy in thermodynamic predictions and optimized call parameters was reduced somewhat, owing to dependence on the effective U parameter [31]. Therefore, the calculations of formation energy using the DFT+U method will only give trends in energy changes.**

The doped systems were constructed from 3×3×1 108-atom anatase supercells. The F atom was substituted for an O atom and the Zr atom for a Ti atom, **corresponding to 0.93% dopant concentration.** F/Zr-codoped anatase was modeled by a single substitution of F for one O atom, and either one adjacent or the furthest Ti atom was replaced by substitution of a Zr atom per supercell (Zr(A) for furthest away). The free energy of this 'furthest-away' optimized configuration was evaluated to be some 0.1eV lower than the next lowest total-energy optimized configuration, in which the F and Zr dopant atoms were nearest to each other (Zr(B)); a variety of different co-doping placement strategies were attempted. Additionally, one of the oxygen atoms was removed to create to an oxygen vacancy in the F and/or Zr doped system. The supercell model is shown in Figure 1.

3. Results and Discussion

3.1 Evaluation of the Effective U value

Although GGA+U approach can improve the band gap partially and describe the electronic structure of semiconductors more reliably, the main limitation is that the calculated results depend highly on the U values. So, it is necessary to select U values tentatively to seek good agreement of the calculated properties with the experimental results. In our calculations, we have selected the cases of F-doped TiO_2 and the removal of oxygen vacancy in TiO_2 to test the U values owing to the existence of Ti 3d states induced by F and the presence of an oxygen vacancy in the band gap of host materials. Here, a series of U values of 4.0, 4.5, 5.0, and 6.3 eV were used on the Ti 3d states. The calculated density of states (DOS) and projected density of states (PDOS) of TiO_2 with oxygen vacancy and F dopant are plotted in Figs 2 and 3, respectively. Comparing Fig. 2 with Fig.3, it was found that U = 6.3 eV yields a correct description of the electronic structures of both systems. The reasons are as follows: 1) oxygen vacancies will induce small spin-polarization in anatase TiO_2, as shown by Kim et al. [32]; 2) oxygen vacancies as well as F dopants will induce Ti 3d states into the band gap of TiO_2. [20]; 3) the calculated band gap of 3.0 eV is close to 3.14 eV in our previous work using GGA optimized geometry [22] and the experimental value (3.2 eV). Therefore, U = 6.3 eV was used on Ti 3d states in the present work. A detailed discussion of electronic structures of F-doped TiO_2 will be presented in part 3.3 B.

3.2 Energetic and electronic properties of stoichiometric TiO_2

3.2 A Formation Energies

The formation energy is an important criterion to evaluate the relative difficulty for the incorporation of dopants into the host lattice. This also determines the relative stability of the doped systems. The formation energies of substitutional F, Zr, and F/Zr dopants were calculated by

$$E_{form} = E(doped) - E(Ti_{36}O_{72}) - \mu_F + \mu_O \quad (1)$$

$$E_{form} = E(doped) - E(Ti_{36}O_{72}) - \mu_{Zr} + \mu_{Ti} \quad (2)$$

$$E_{form} = E(doped) - E(Ti_{36}O_{72}) - \mu_F - \mu_{Zr} + \mu_O + \mu_{Ti} \quad (3)$$

where $E(doped) = E(Ti_{36}O_{71}F)$, $E(Ti_{35}ZrO_{72})$, $E(Ti_{35}ZrO_{71}F)$ are the total energies of supercells containing the F, Zr, or F/Zr impurities, respectively, while $E(Ti_{36}O_{72})$ is the total energy of the pure anatase supercell. μ_F and μ_{Zr} denote the chemical potentials of the impurity F and Zr, respectively. μ_O (μ_{Ti}) is the chemical potential for O (Ti). The formation energies for the different doped systems vary as a function of the oxygen chemical potential, which characterizes the oxygen environment during synthesis [20, 33]. The environment acts as a reservoir, which can give or take any amount of oxygen without changing temperature and pressure [34]. Low values of μ_O correspond to O-poor growth conditions, while high values of μ_O correspond to O-rich conditions. By referencing μ_O to the energy of an O atom in an O_2 molecule ($\mu_O = \mu(O_2)/2 + \mu_O^{'}$), here we take $-4eV \le \mu_O^{'} \le 0eV$, where the value $\mu_O^{'}$ = 0 corresponds to the O-rich limit whereas $\mu_O^{'}$ = -4 eV is approximately half of the enthalpy of formation of anatase TiO_2 [35]. The chemical potential of Ti is calculated from $\mu_{Ti} = \mu(TiO_2) - 2\mu_O$. For F and Zr impurities, the chemical potentials μ_F are determined by $\mu_F = \frac{1}{2}\mu(F_2)$. μ_{Zr} is calculated based on consideration of cubic

ZrO_2, using the relationship $\mu_{Zr} = \mu(ZrO_2) - \mu(O_2)$. The calculated formation energies are plotted in Figure 4. Examination of these results suggests that: 1) F prefers to occupy O sites under Ti-rich growth conditions while Zr prefers to substitute for Ti under O-rich conditions; 2) codoping of F with Zr promotes F incorporation and the values of Zr@Ti and FZr@OTi are close to each other under O-rich growth conditions. Further, O-rich growth conditions correspond to the sol-gel synthesis conditions used to fabricate the TiO_2 sample. Therefore, the synthesis of F/Zr-codoped TiO_2 may be realised experimentally, albeit after overcoming a substantially larger energy barrier in comparison to single-Zr doping under O-rich growth conditions**.** The optimized geometries indicate that doping with F and/or Zr induces a local lattice distortion around the dopant atoms because the ionic radii are somewhat different between O^{2-} (1.21 Å) and F^- (1.33 Å), as well as between Ti^{4+} (0.61 Å) and Zr^{4+} (0.72 Å) [35]. For example, the optimized F-Ti bond lengths are 2.169 and 2.059 Å in the F@O case, which are elongated by about 0.157 and 0.077 Å vis-à-vis O-Ti bond lengths in pure anatase (2.012 and 1.982 Å). For the Zr@Ti case, the optimized O-Zr bond lengths are 2.148 and 2.076 Å, which also increased by 0.116 and 0.094 Å relative to O-Ti bond lengths in pure anatase. At the same time, F-, Zr- and F/Zr-doping actually resulted in an expansion of the system volume as well as surface area: the volumes were 1300.80, 1303.48, 1308.25, 1311.68 and 1311.39 $Å^3$ for pure, F@O, Zr@Ti, FZr@OTi(A) and FZr@OTi(B) structures, respectively. This small difference between FZr@OTi(A) and FZr@OTi(B) serves also to explain why the latter case is 0.1 eV higher in formation energy than the former.

3.2 B Electronic Properties

Before studying the electronic structures of F- and Zr-monodoped anatase, we should consider the electronic structure of pure anatase. Hence, we calculated the density of states (DOS) and projected density of states (PDOS) (cf. Figs. 5a and a') and they show that O 2p states dominate the valance band, while Ti 3d states are located mainly in the conduction band. It may be expected that F and Zr modify the conduction and valence bands to a greater and lesser extent, respectively, because of their different p and d orbital characters.

For F-doped anatase (cf. Figs. 5b and b'), substitution of F at the host O site acts as a single donor due to F having one more electron than O, which reduces a Ti^{4+} ion to Ti^{3+}. Further, the reduced Ti 3d states located below the conduction band **minimum** (CBM) of the host TiO_2 are responsible for the band gap narrowing, which has reported previously by Czoska et al. [20] using hybrid functional calculations. However, this conclusion is not consistent with previous LDA and GGA calculations [8, 19] which have revealed the absence of intermediate energy levels in the band gap, indicating that DFT+U is necessary to describe correctly the electronic properties of F-doped TiO_2. One may expect that replacement O by F will lead to strong hybridization between F 2p and Ti 3d states because the electronegativity of F is larger than that of O; this would lead to F 2p orbitals residing well into the valence band. However, DFT (either LDA or GGA) cannot describe correctly the strong interaction of F-Ti pairs and can induce artificial electronic structure. The Bader

charge [36] on F is -0.83 |e| and this value approximates -1 |e|, which indicates that the most likely conformation of F is as the F^- ion.

For Zr-doped TiO_2 (cf. Figs. 5c and c'), it was found that there is neither band gap narrowing nor the occurrence of defect levels in the band gap. The Zr 4d states reside in the conduction and valence bands with the formation of anti-bonding and bonding states, respectively; this is consistent with previous theoretical and experimental work [37]. This shows clearly that Zr doping cannot improve band gap-dependent electronic properties, such as photocatalytic activity. One may rationalise that the replacement of Ti by Zr induces only a slight increase in the bond lengths of the inner coordination shells and that the ZrO_6 still retain an octahedral geometry. Furthermore, we have also evaluated Bader charges to compare the ionic characters of the different bonds. That of the Zr atom is 3.52 |e| **and approaches 3.43|e| in pure ZrO_2**, which indicates that almost all Zr valence electrons transfer to adjacent O atoms with the formation of highly ionic bonds.

For F/Zr-codoped anatase, the formation energies of the two configurations are very close, as shown in the Figure 4. Hence, a comparison of the electronic structures of the FZr@OTi(A) and FZr@OTi(B) is both merited and interesting. The DOS and PDOS are shown in Figure 6. For the FZr@OTi(A) system (cf. Figs. 6 a and a'), an isolated Ti 3d state induced by F locates in the band gap, which is beneficial for electron transition either from the valence band maximum (CBM) to the conduction band minimum (CBM) or from the gap states to the CBM. For the FZr@OTi(B) model (cf. Figs. 6b and b'), although formation of an F-Zr atomic pair takes place,

one more electron is still transferred from the F dopant to its adjacent Ti atom due to the larger electronegativity of Ti (1.54) relative to Zr (1.33) [35]. In this case, Ti 3 d gap states are induced also from the F dopant. that the expansion in volume and surface area upon codoping are two key factors which influence photocatalytic activity and these serve as a possible explanation of the experimentally observed higher photo-activity of codoped systems vis-à-vis modoping cases under UV irradiation [21]. The Bader charges on F and Zr were found to be -0.83 |e| and 3.52 |e|, respectively, almost the same value as in F- and Zr-doped anatase. Hence, the F-Ti and O-Zr bonds still retain their ionic bond characteristics.

3.3 Energy and electronic properties of doped non-stoichiometric TiO_2

3.3 A Formation energy

The oxygen vacancy is the main lattice defect. In particular, the incorporation of slightly larger F^- and Zr^{4+} ions into the anatase lattice could feasibly create oxygen vacancies, and this has been confirmed by previous experimental studies [21, 37]. Hence, the two main aims of this study of doped non-stoichiometric anatase are to investigate whether the dopants (F and Zr) promote the creation of an oxygen vacancy and to assess the influence on electronic properties due to the interplay between an oxygen vacancy and the dopants. The formation energy for the creation of a single vacancy is calculated based on equation (4):

$$E_{form} = E(Ti_{36}O_{71}) - E(Ti_{36}O_{72}) + \mu_O \quad (4)$$

where $E(Ti_{36}O_{71})$ is the total energy of the system containing one oxygen vacancy in

the pure (undoped) case. The formation energy for the creation of a single oxygen vacancy is 4.96 eV in the case of an 108-atom supercell calculation, which is comparable to thermogravimetric experimental results of 3.9 eV [38] and 5.6 eV [39] and a previous DFT study result of 4.18 eV for a 162-atom calculation [40]. However, the formation energies were reduced to **3.9**, **4.05**, **4.15** and **4.25** eV in the presence of F-, Zr-, F/Zr(B)-, and F/Zr(A)-dopants, respectively, according to the formula

$$E_{form} = E(Ti_{36}O_{70}F) - E(Ti_{36}O_{71}F) + \mu_O \quad (5)$$

$$E_{form} = E(Ti_{35}ZrO_{71}) - E(Ti_{35}ZrO_{72}) + \mu_O \quad (6)$$

$$E_{form} = E(Ti_{35}ZrO_{70}F) - E(Ti_{35}ZrO_{71}F) + \mu_O \quad (7)$$

This indicates that doping can create oxygen vacancies relatively easily. It was confirmed experimentally that doping created oxygen vacancies in the samples [21]. In addition, the formation energies of F-, Zr- and F/Zr-doped TiO_2 in the presence of oxygen vacancies are plotted in Figure 7 based on the formula:

$$E_{form} = E(doped) - E(Ti_{36}O_{71}) - \mu_F + \mu_O \quad (8)$$

$$E_{form} = E(doped) - E(Ti_{36}O_{71}) - \mu_{Zr} + \mu_{Ti} \quad (9)$$

$$E_{form} = E(doped) - E(Ti_{36}O_{71}) - \mu_F - \mu_{Zr} + \mu_O + \mu_{Ti} \quad (10)$$

where $E(doped)$ represents the total energy of $E(Ti_{36}O_{70}F)$, $E(Ti_{35}O_{71}Zr)$, and $E(Ti_{35}O_{70}FZr)$ (A, B), respectively. Compared with Fig.4, this shows that oxygen vacancies are beneficial for incorporation of dopants into the lattice. Hence, the oxygen vacancies play an important role governing the electronic structures of these doped systems, so some discussion of this is necessary.

3.3 B Electronic Structures

Before discussing the electronic properties of the different (doped and co-doped) systems in the presence of oxygen vacancies, it is instructive to investigate the electronic structure of a single oxygen vacancy present in the anatase lattice. The calculated DOS and PDOS of the oxygen vacancy compared to pure TiO_2 is shown in Figure 8. The removal of one oxygen atom leads to two adjacent Ti atoms in the formation of "Ti^{3+}", which creates one impurity **state** in the middle of the band gap as well as another state delocalized into the conduction band, as shown in Figure 3 (with U = 6.3 eV). Hence, oxygen vacancies can improve photocatalytic activity under visible-light irradiation. This agrees well with previous DFT + U calculations and experiments [41, 42]. The DOS and PDOS for doped anatase with an oxygen vacancy are shown in Figure 8, for F@O-O_v, Zr@Ti-O_v, FZr@OTi(A)-O_v, FZr@OTi(B)-O_v and FZr@OTi(A)-O_v. For the F@O-O_v system (cf. Fig.8 a&a'), there are more impurities than those of F@O in stoichometric TiO_2 because one oxygen vacancy will create two new "Ti^{3+}" gap states. Due to its slightly smaller band gap, it is expected that F-doped TiO_2 in the presence of oxygen vacancies exhibits better photocatalytic activity than F-monodoped TiO_2. For the Zr@Ti-O_v system (cf. Fig.8 b&b'), it can be seen clearly that the impurity states arise mainly from Ti 3d rather than Zr 4d, and hence the higher photocatalytic activity of Zr-doped TiO_2 is due to the incorporation of Zr inducing oxygen vacancies via the formation of kinds of "Ti^{3+}". For F/Zr-codoped systems, we selected FZr@OTi(A)-O_v to analyse the electronic structure due to the similar electronic structures FZr@OTi(B)-O_v. As shown in Fig.8

c&c', there are substantially more Ti^{3+} 3d gap states than for the FZr@OTi(A) configuration without an oxygen vacancy. The presence of these impurity states would be expected to lead to improved photo-excited electron transfer. This implies that the FZr@OTi(A) motif would exhibit greater photocatalytic activity in the presence of oxygen vacancies, and this is consistent with experimental reports [21].

4. Conclusions

We have calculated the energetic and electronic properties of F-, Zr, and F/Zr-doped anatase TiO_2, as well as considered the interplay between these systems and the presence of oxygen vacancies, by means of density functional theory using the GGA + U approach. The calculated formation energies suggest that the presence of F, Zr, and F/Zr are energetically favourable towards the creation of oxygen vacancies and codoping leads to expansion of the volume of the host lattice. The electronic structures indicate that F-monodoping **reduces** one adjacent Ti^{4+} to Ti^{3+} and **the 3d states of Ti^{3+} ion are located** in the band gap, while Zr-monodoping does not induce an appreciable change in the band gap and thus would not contribute to greater photo-activity. In particular, F and Zr co-doping can serve to enhance photocatalytic activity under UV irradiation due to creation of oxygen vacancies, which serves to rationalise recent experimental findings of these effects [21].

Acknowledgements

This work was supported by the Irish Research Council for Science, Engineering and

Technology (IRCSET). The authors thank the Irish Centre for High End Computing and Science Foundation Ireland for the provision of computational resources.

References

(1) Linsebiger, A. L.; Lu, G. Q.; Yates, J. T. *Chem. Rev.* ***1995***, *95*, 725.

(2) Fujishima, A.; Honda, K. *Nature* ***1972***, *28*, 37.

(3) Herrmann, J. M.; Disdier, J.; Pichat, P. *Chem. Phys. Lett.* ***1984***, *108*, 618.

(4) Choi, W.; Termin, A.; Hoffmann, M. R. *J. Phys. Chem.* ***1984***, *98*, 13669.

(5) Yamashita, Y.; Ichiashi, M.; Taeuchi, S.; Kishiguchi, M.; Anpo, J. *Synchrotron Radiat.* ***1999***, *6*, 451.

(6) Wang, Y. Q.; Cheng, H. M.; Zhang, L. et al., *J. Mol. Catal. A* ***2000***, *151*, 205.

(7) Long, R.; Dai,Y.; Huang, B. B. *Comput. Mater. Sci.* ***2009,*** *45*, 223.

(8) Asahi, R.; Morikawa, T.; Ohwaki,T.; Aoki, K.; Taga,Y. *Science* ***2001***, *293*, 269.

(9) Umebayashi, T.; Yamaki, Y.; Itoh, H.; Asai, K. *Appl. Phys. Lett.* ***2002***, *81*, 454.

(10) Umebayashi, T.; Yamaki, Y.; Yamamoto, S.; Miyashita, A.; Tanaka, S.; Asai, K. *J. Appl. Phys.* **2003,** *93*, 5156.

(11) Chen, D.; Yang, D.; Wang, Q. Z.; Jiang, Y. *Ind. Eng. Chem. Res.* ***2006***, *45*, 4110.

(12) (a) Sakthivel, S.; Kisch, H. *Angew. Chem., Int. Ed.* ***2003***, *42*, 4908. **(b) Graciani, J.; Nambu, A.; Evans, J.; Rodriguez, J. A. Sanz, J. F.** ***J. Am. Chem. Soc.*** **2008,** ***130,*** **12056.**

(13) Hernandez-Alonso, M. D.; Coronado, J. M.; Bachiller-Baeza, B.; Fernandez-Grarcia, M.; Soria, *J. Chem. Mater.* **2007**, *19*, 4283.

(14) Fu, X. Z.; Clark, L. A.; Yang, Q.; Anderson, M. A. *Environ. Sci. Technol.* ***1996***, *30*, 647.

(15) Yu, J. C.; Yu, J.; Ho, W.; Jiang, Z.; Zhang, L. *Chem. Mater.* 2002, *14*, 3808.

(16) Li, D.; Haneda, H.; Labbsetwar, N.; Hishita, S.; Ohashi, N. *Chem. Phys. Lett.* ***2005***, *401*, 579.

(17) Todorova, N.; Ginnakopoulou, T.; Vaimakis, T.; Trapalis, C. *Mater.Sci. & Eng. B* **2008**, *152*, *50*.

(18) Yamaki, T.; Umebayashi, T.; Sumita, T.; Yamamoto, S.; Maekawa, M.; Kawasuso, A.; Itoh, H. *Nuclear Instruments and Methods in Physics Research B* **2003**, *206*, 254.

(19) Yang, K. S.; Dai, Y.; Huang, B. B. Whangbo, M. H. *Chem. Mater.* **2008**, *20*, 6528.

(20) Czoska,A. M.; Livraghi, S.; Chiesa, M.; Giamello, E.; Agnoli, S.; Granozzi, G.; Finazzi, E.; Valentin, C. Di.; Pacchioni, G. *J. Phys. Chem. C* **2008**, *112*, 8951.

(21) Liu, S. W.; Yu, J. G.; Mann, S. *J. Phys. Chem. C*. **2009**, *113*, 10712.

(22) Long, R.; English, N. J. *J. Phys. Chem. C* **2009**, *113*, 8373.

(23) Long, R.; English, N. J. *Appl. Phys. Lett.* **2009**, *94*, 132102.

(24) Long, R.; English, N. J. *Chem. Phys. Lett.* **2009**, *478*, 175.

(25) Gai, Y. Q.; Li, J. B.; Li, A. S.; Xia, J. B.; Wei, S. H. *Phys. Rev. Lett.* **2009**, *102*, 036402.

(26) Kresse, G.; Hafner, J. *Phys. Rev. B* **1993**, *47*, 558.

(27) Kresse, G.; Furtherműller, J. *Phys. Rev. B* **1996**, *54*, 11169.

(28) Perdew, J. P.; Burk, K.; Ernzerhof, M. *Phys. Rev. Lett.* **1996**, *77*, 3865.

(29) Monkhorst, H. J.; Pack, J. D. *Phys. Rev. B* **1976**, *13*, 5188.

(30) Dudarev, S. L.; Botton, C. A.; Savarsov, S. Y.; Hunphreys, C. J.; Sutton, A. P.

Phys. Rev. B **1998**, *57*, 1505.

(31) **Loschen, C.; Carrasco, J.; Neyman, K. M.; IIIas, F. *Phys. Rev. B* 2008, *75*, 035115.**

(32) Kim, D.; Hong, J. S.; Park, Y. R.; Kim, K. J.; *J. Phys.: Condens. Matter* **2009**, *21*, 195405.

(33) Valentin, C. Di.; Pacchioni, G.; Selloni, A. *Chem. Mater.* **2005**, *17*, 6656.

(34) Reuter, K.; Scheffler, M. *Phys. Rev. B* **2001**, *65*, 035406.

(35) CRC Handbook of Chemistry and Physics 87th ed.; Lide, D. R. Taylor & Francis: London, 2006.

(36) Sanville, E.; Kenny, S. D.; Smith, R.; Henkelman, G. *J. Comp. Chem.* **2007**, *28*, 899.

(37) Lippens, P. E.; Chadwick, A. V.; Weibel, A.; Bouchet, R.; Knauth, P. *J. Phys. Chem. C* **2008**, *112*, 43.

(38) Forland, K. S. 1959 Tionde Nordiske Kemistmotet (Stockholm: Almqvist)

(39) Forland, K. S. *Acta Chem. Scand.* **1964**, *18*, 1267.

(40) Keith, J. B.; Wang, H.; Fultz, B.; Lewis, J. P. *J. Phys.: Condens. Matter* **2008**, *20*, 022202.

(41) Finazzi, E.; Valentin, C. Di.; Pacchioni, G.; Selloni, A. *J. Chem. Phys.* **2008**, *129*, 154113.

(42) Henderson, M. A.; Epling, W. S.; Peden, C. H. F.; and Perkins, C. L. *J. Phys. Chem. B* **2003**, *107*, 534.

Figure Captions

Figure 1. Supercell model for F/Zr-doped anatase showing the location of the dopants. The ion doping sites are marked with F and Zr. The large light balls and the small red balls represent the Ti and O atoms, respectively.

Figure 2. The density of states (DOS) and Ti 3d projected density of states (PDOS) for anatase TiO_2 in the presence of one oxygen vacancy with U = 4.0, 4.5 5.0 and 6.3 eV.

Figure 3. The density of states (DOS) and Ti 3d projected density of states (PDOS) for F-doped anatase TiO_2 with U = 4.0, 4.5 5.0 and 6.3 eV.

Figure 4 Formation energies (eV) E_{form} as a function of the oxygen chemical potential for F@O, Zr@Ti, FZr@OTi(A) (solid line) and FZr@OTi(B) (dotted line).

Figure 5. The density of states (DOS) and projected density of states (PDOS) for each monodoped system. The top of the valence band of pure anatase is taken as the reference level.

Figure 6. The density of states (DOS) and projected density of states (PDOS) for FZr@OTi(A) and FZr@OTi(B) systems. The top of valence band of pure anatase is taken as the reference level.

Figure 7 Formation energies (eV) E_{form} as a function of the oxygen chemical potential

for F@O-O_v, Zr@Ti-O_v, FZr@OTi(A)-O_v (solid line) and FZr@OTi(B)-O_v (dotted line).

Figure 8 DOS for F@O, Zr@Ti, and FZr@OTi(A) (solid line) compared with pure TiO_2 (not shown here) and PDOS for F 2p (red), Zr 4d (black) and Ti 3d (green) states.

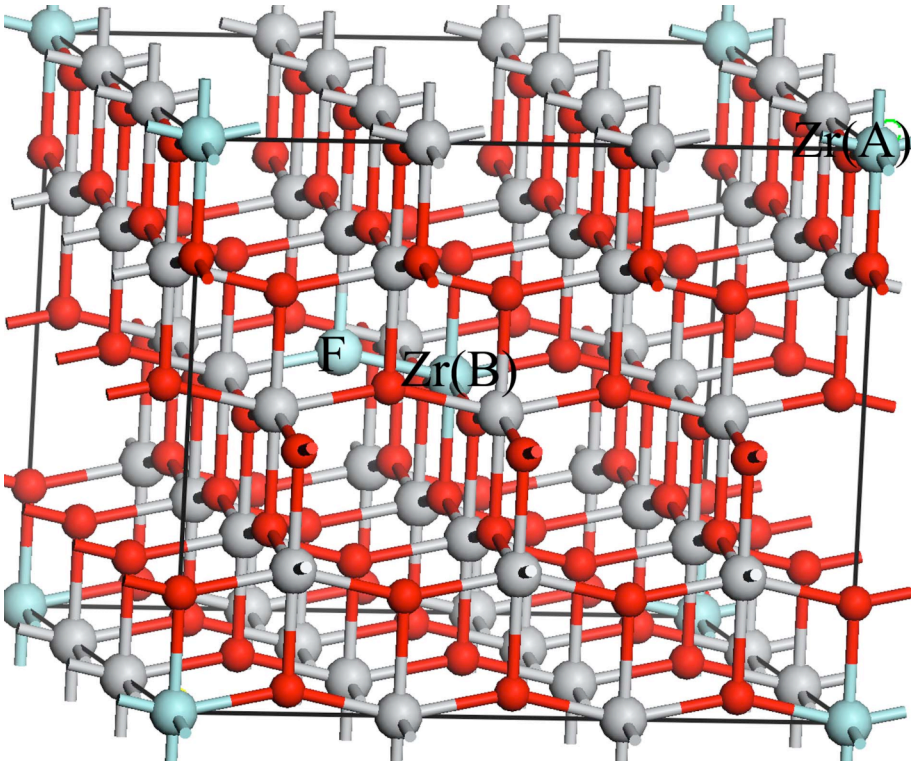

Figure 1

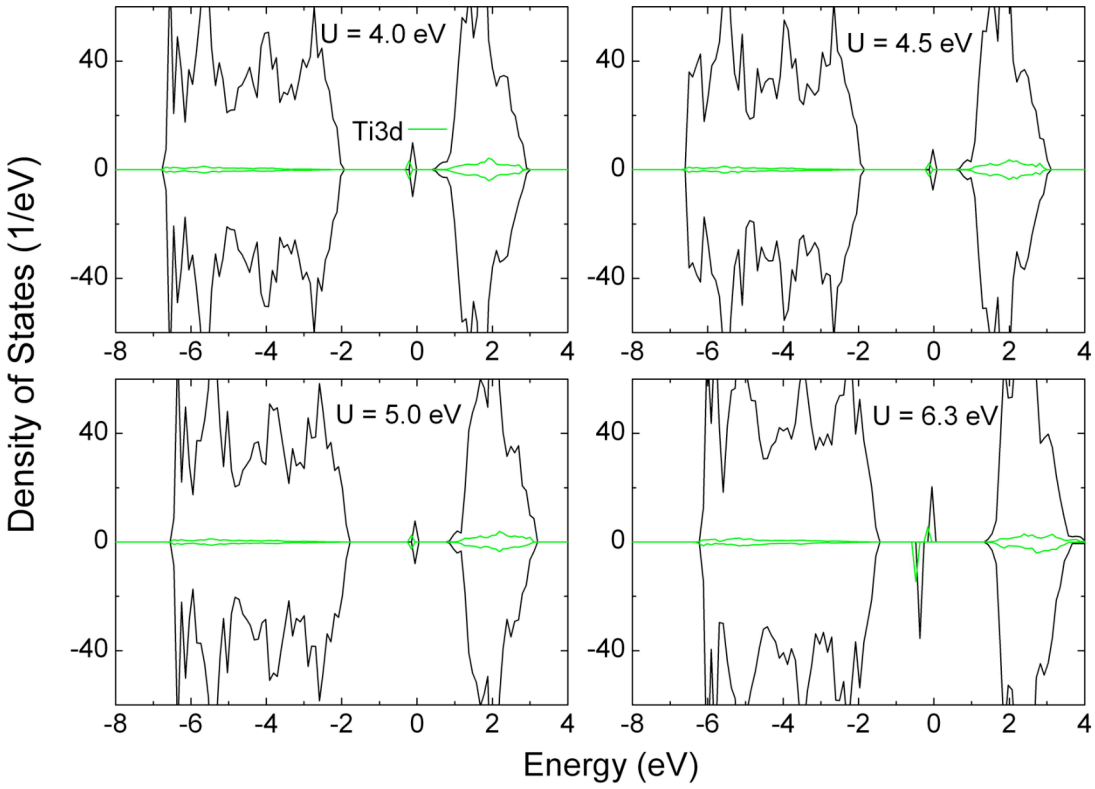
U = 4.0 eV
Ti3d
U = 4.5 eV
U = 5.0 eV
U = 6.3 eV
Density of States (1/eV)
Energy (eV)
40
0
-40
-8
-6
-4
-2
0
2
4

Figure 2

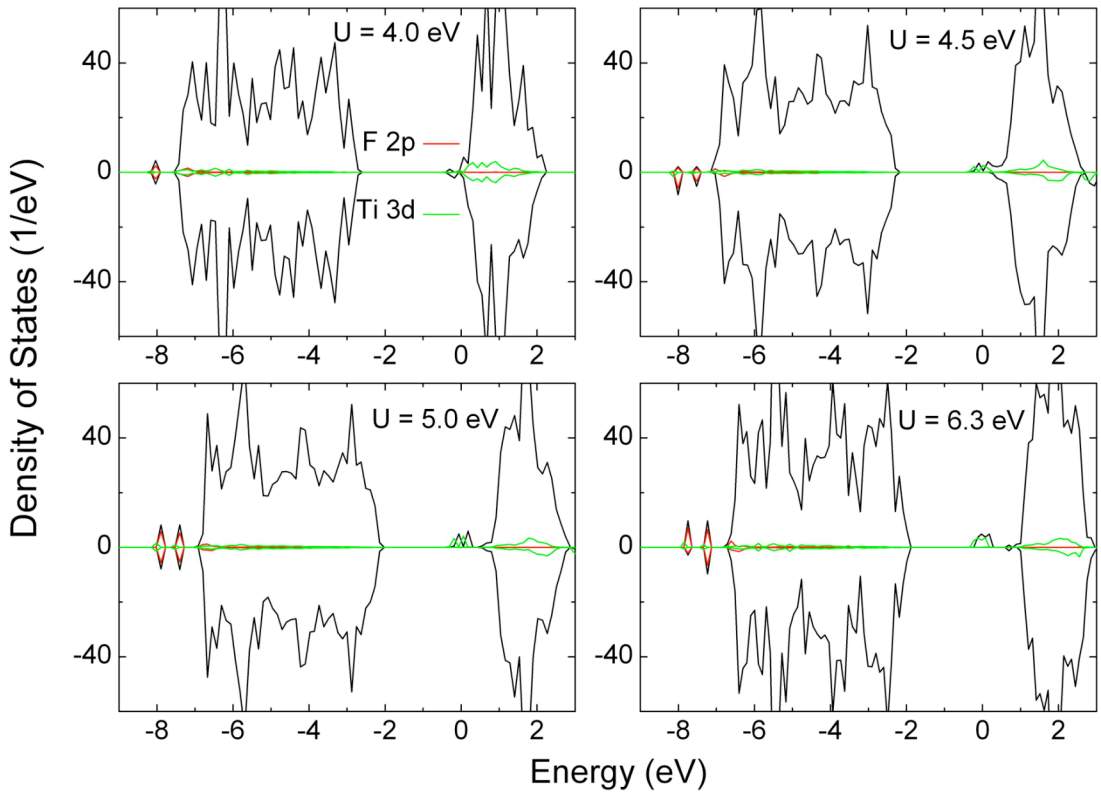
U = 4.0 eV
F 2p
Ti 3d
U = 4.5 eV
U = 5.0 eV
U = 6.3 eV
Density of States (1/eV)
Energy (eV)
40
0
-40
-8
-6
-4
-2
0
2

Figure 3

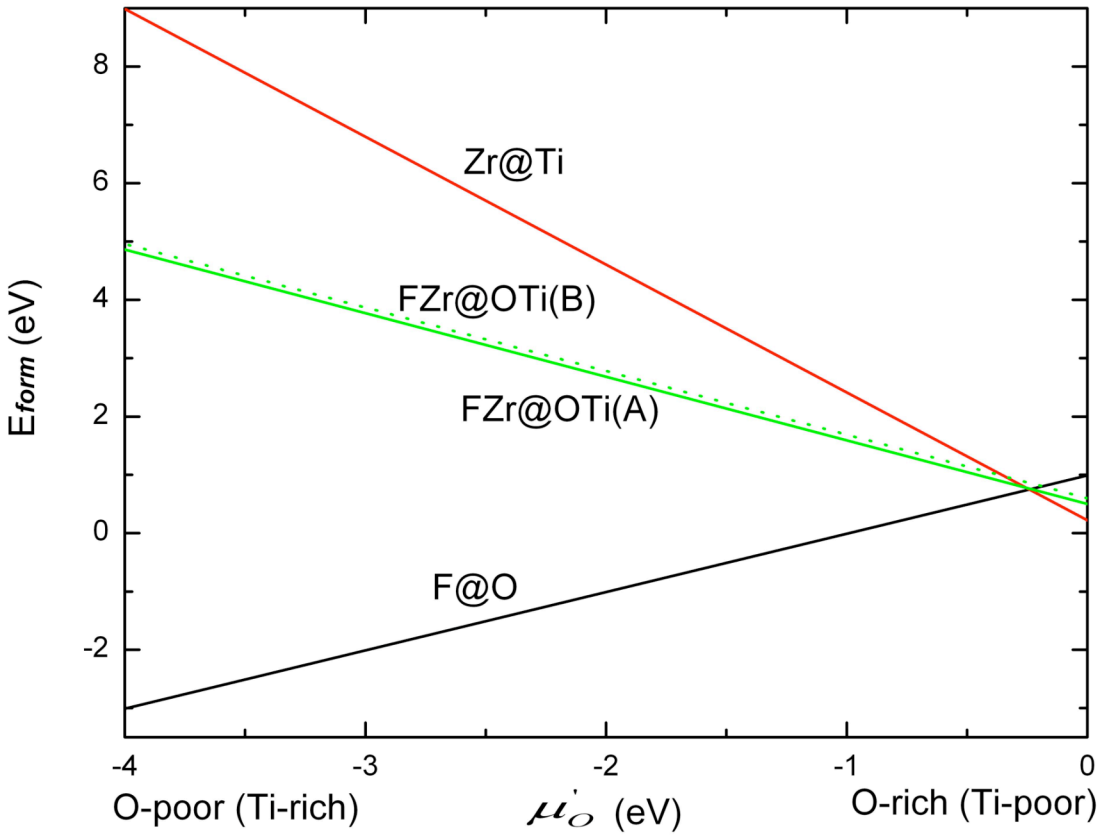
8
6
4
2
0
-2
E*form* (eV)
Zr@Ti
FZr@OTi(B)
FZr@OTi(A)
F@O
-4
-3
-2
-1
0
O-poor (Ti-rich)
μ_O' (eV)
O-rich (Ti-poor)

Figure 4

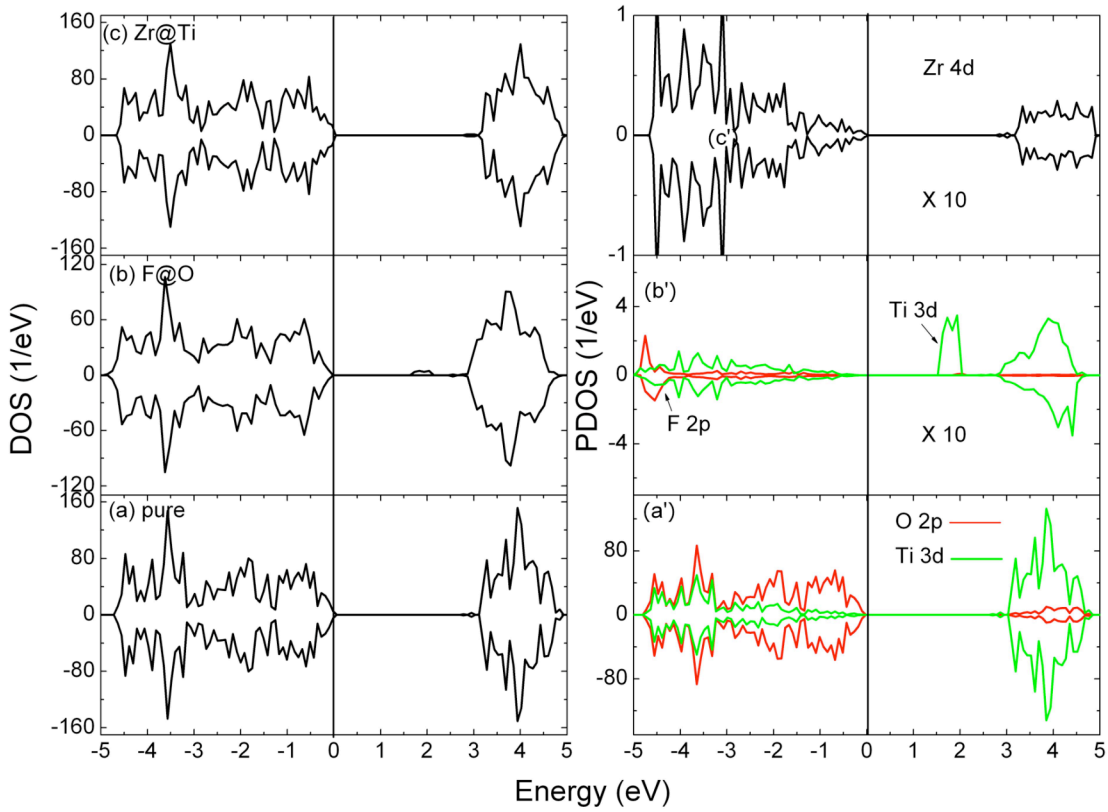
(c) Zr@Ti
(b) F@O
(a) pure
DOS (1/eV)
(c')
Zr 4d
X 10
(b')
Ti 3d
F 2p
X 10
(a')
O 2p
Ti 3d
PDOS (1/eV)
Energy (eV)

Figure 5

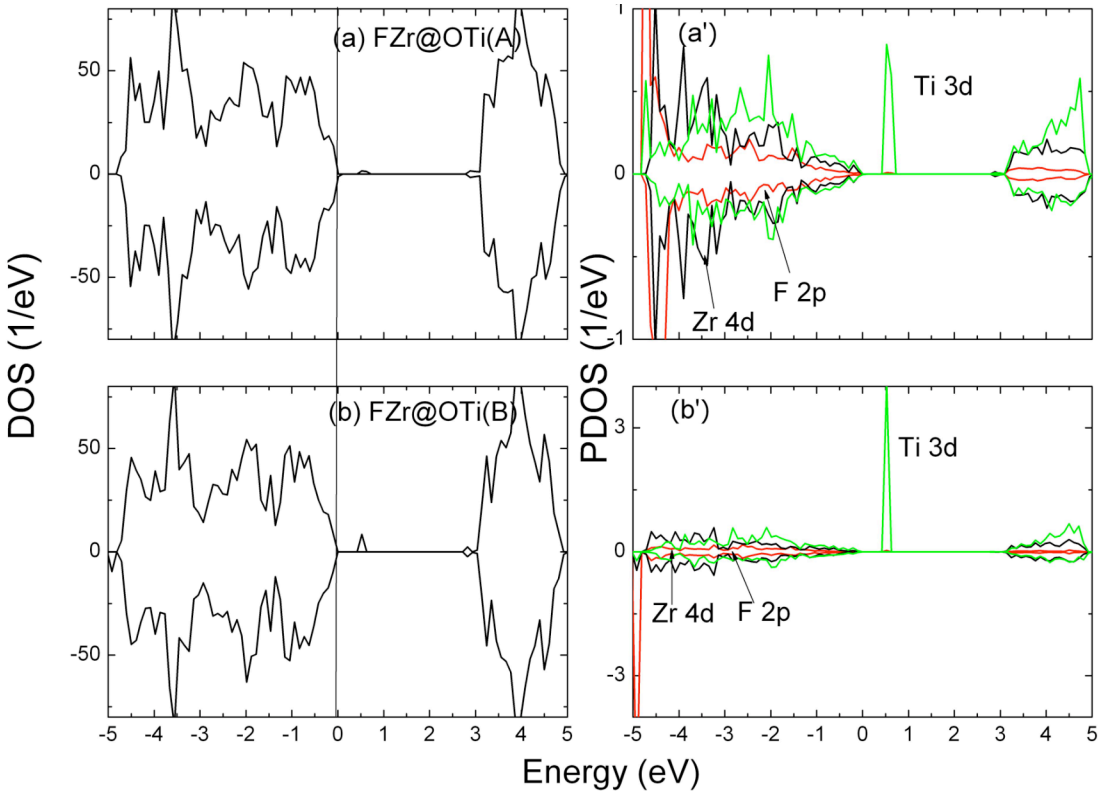
(a) FZr@OTi(A)
(b) FZr@OTi(B)
(a')
(b')
Ti 3d
F 2p
Zr 4d
DOS (1/eV)
PDOS (1/eV)
Energy (eV)

Figure 6

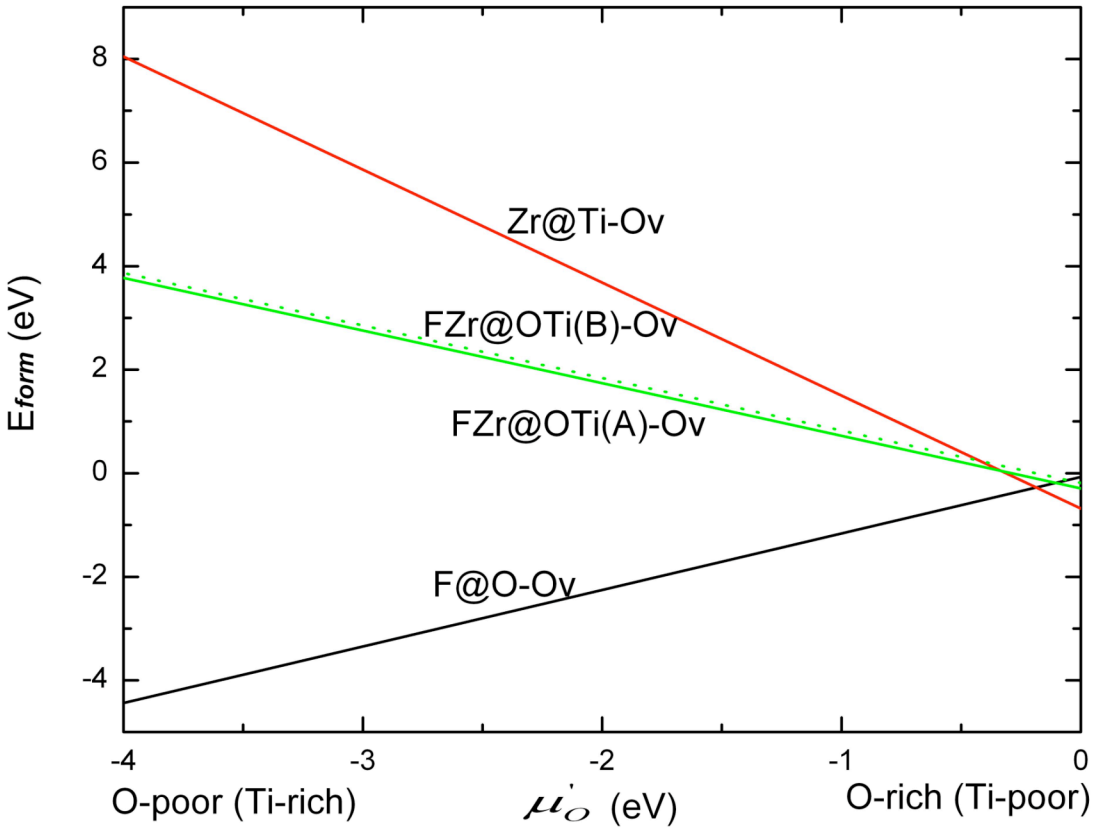
8
6
4
2
0
-2
-4
E*form* (eV)
Zr@Ti-Ov
FZr@OTi(B)-Ov
FZr@OTi(A)-Ov
F@O-Ov
-4
-3
-2
-1
0
O-poor (Ti-rich)
μ_O' (eV)
O-rich (Ti-poor)

Figure 7

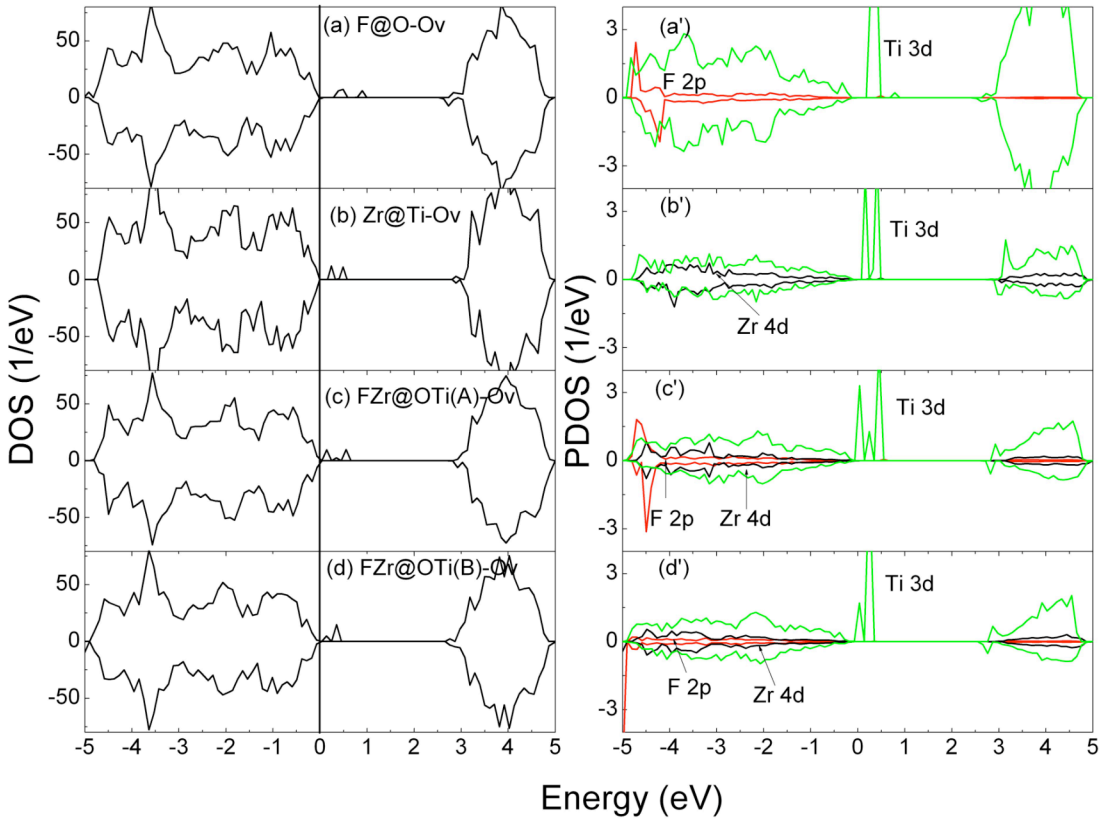
(a) F@O-Ov
(b) Zr@Ti-Ov
(c) FZr@OTi(A)-Ov
(d) FZr@OTi(B)-Ov
DOS (1/eV)
(a')
(b')
(c')
(d')
Ti 3d
F 2p
Zr 4d
PDOS (1/eV)
Energy (eV)

Figure 8